Sensitive Analysis of Passive Dehumidification System using Solar Heat

Haksung Lee[1], Akihito Ozaki[2], Myonghyang Lee[3]

[1]Graduate student, Kyushu University, Fukuoka, Japan
[2]Professor, Kyushu University, Fukuoka, Japan
[3]Associate Professor, Ritsumeikan University, Kyoto, Japan

Abstract

A passive dehumidification and solar collector (PDSC) system is proposed as a possible means of controlling thermal loads. Research was conducted to develop the thermodynamic-potential-based fundamental principle of the PDSC. This work will enable the combined analysis of heat and moisture movement in PDSC envelope systems. The quantitative simulation and experimental results indicate that significant latent heat reduction can be achieved by employing PDSC systems, which will reduce the energy consumptions of indoor temperature and humidity control systems by using solar energy.

Introduction

The current energy conservation standards demand quantitative evaluation; however, quantitative analysis of passive natural energy collection methods has not been performed. In particular, construction methods, which significantly influence latent heat loads, have been ignored, as have moisture absorption and desorption (indoor humidity variations). Furthermore, indoor environment control is strongly dependent on airtightness and equipment such as air conditioners and dehumidifiers; thus, high initial and running costs are imposed. Currently, about 30%–40% of residential energy consumption is used for cooling and heating (METI, 2014). Therefore, a passive dehumidification and solar collector (PDSC) system that can control thermal loads using solar energy collected from the external walls and roofs of buildings is proposed in this paper. The system can reduce latent heat loads in summer by dehumidification and maintain low heat loads in winter by collecting solar energy.

A number of reports have presented analyses of desiccant dehumidification techniques (Mazzei et al., 2005). Areemit and Sakamoto (2006) proposed a building design with a passive dehumidification system by using the sorption properties of a wooden attic space. Substantial research on air dehumidification with mechanical equipment, which requires significant capital investment and the use of degradable chemical desiccants, was conducted, while little research on passive air dehumidification using building components has been performed. Natural fiber materials such as kenaf cores (Misha, 2014) and artificial fiber materials (Zhang, 2011) such as hollow fiber membranes have exhibited excellent dehumidification performances.

The proposed PDSC system can perform dehumidification all day, via an air circulation system using a ventilation layer inside a wall combined with hygroscopic cellulose fiber (CF) insulation. The excellent performance of CF insulation was verified previously (Lee et al., 2016). In this paper, the thermodynamic-potential-based fundamental principle of the PDSC envelope system, which was designed to reduce latent heat loads via dehumidification during the summer, is described. Analysis of the behavior of the water potential in the summer and the results of a laboratory experiment performed for verification are also provided. Moreover, the effectiveness of the PDSC envelope system is demonstrated by presenting the results of parameter sensitivity analysis conducted using Hygrabe simulation software for hygrothermal analysis of building envelopes.

PDSC system

System overview

Water potential (Ozaki and Watanabe, 1996) is a type of non-equilibrium thermodynamic energy that is a function of the water vapor concentration, the internal energy of the water vapor molecules, the force acting on the water vapor molecules (adhesive power or capillary action), and the field energy (stresses such as external forces), among other factors. It is analogous to a chemical potential, which is an index of mass equilibrium, for moisture. Figure 1 shows the principal relations between water potential (left y-axis), temperature (x-axis), relative humidity (diagonal lines from the lower left to the upper right), and absolute humidity (downward to the right) (Ozaki, 2005). The water potential at a certain temperature and humidity is given by the sum of the saturated and unsaturated water potentials. The saturated water potential is a type of thermodynamic energy possessed by saturated humid air at a certain temperature.

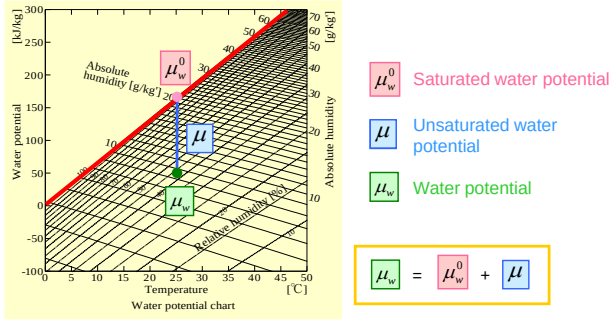

Figure 1: Water potential.

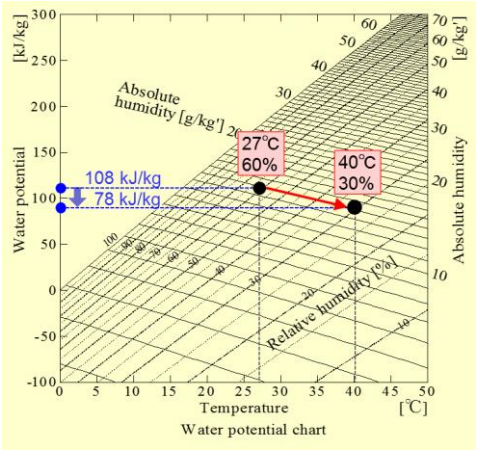

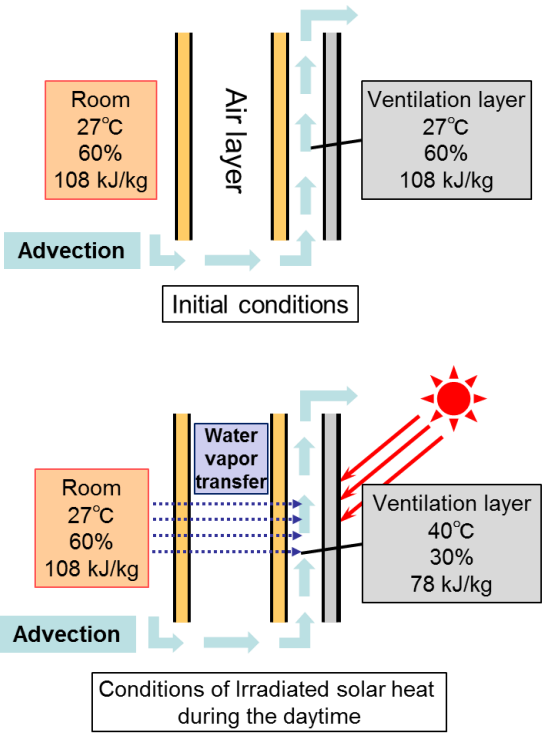

Figure 2: Water potential in the PDSC system during the daytime.

The unsaturated water potential is a type of negative energy indicating the extent of dryness relative to the saturated state. If the absolute humidity changes constantly, the water potential difference between the saturated and unsaturated states increases as the temperature increases (because the relative humidity decreases and the air becomes dry), so the water potential becomes smaller than its initial value. Thus, dry air has a low thermodynamic energy (high potential to contain water vapor), and moisture flow from high-humidity air occurs. Therefore, if the deviation from the equilibrium state (homogeneous state) of the water potential is considered to drive the moisture flow, the water potential difference between the room and inside the wall drives the moisture flow in the PDSC envelope system, resulting in dehumidification.

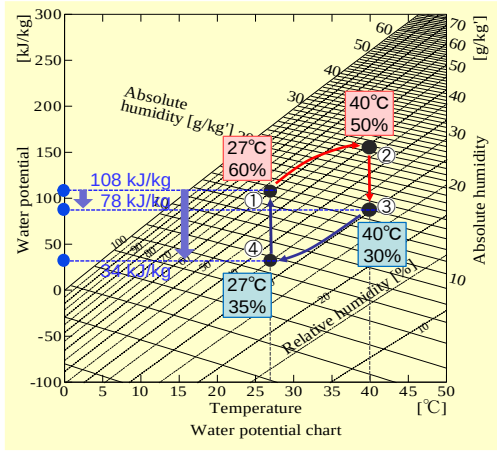

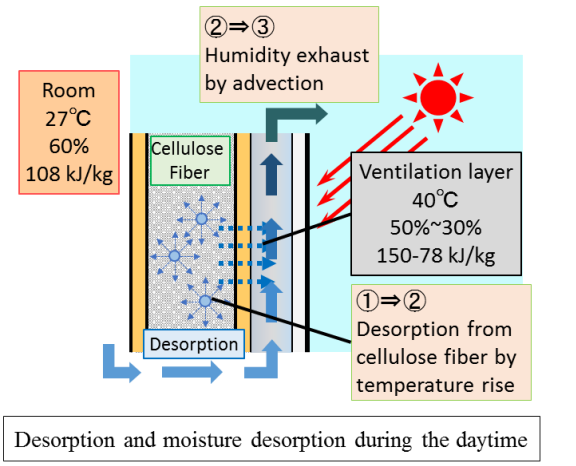

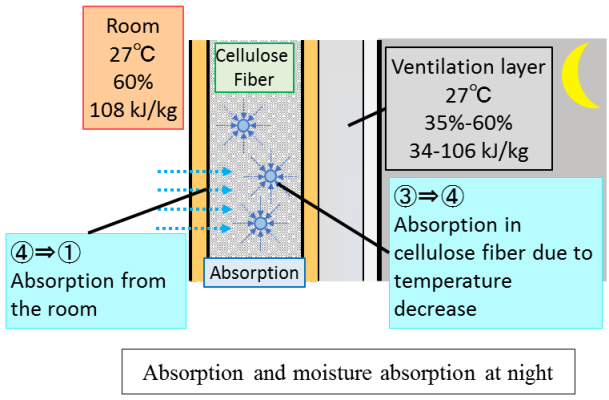

Figure 3: Cycle of moisture absorption and desorption in the summer.

To simplify the explanation of the PDSC envelope system, the advection from the room to the outside air through the ventilation layer is addressed for an external wall composed only of moisture-permeable face material without moisture absorption and desorption properties, as illustrated in Figure 2. On a summer night, if the initial conditions are 27°C and 60% relative humidity inside the room and 27°C outside the room, the wall exists in constant hygrothermal conditions. Then, if the temperature of the ventilation layer reaches 40°C due to irradiation by solar heat during the daytime and moisture desorption from the face material does not occur, the

absolute humidity of the ventilation layer becomes the same as that in the room since indoor air flows into the ventilation layer. However, for the above reasons, the water potential is lower in the ventilation layer than in the room. Therefore, a difference in water potential occurs between the room and the ventilation layer, and moisture flows from the room into the ventilation layer. This is the basic concept of the summer dehumidification process of the PDSC envelope system.

Figure 3 depicts the changes in temperature, humidity, and water potential in the ventilation layer that were obtained by considering the external wall to contain fibrous (CF) insulation between the interior material and the ventilation layer. Ignoring the advection through the ventilation layer (circulation of air from the room through the ventilation layer to the outside) that occurs because of the desorption and diffusion of water vapor from the fibrous insulation material that result from the increase in temperature due to irradiation by solar heat during the daytime, the absolute humidity of the ventilation layer increases to the same extent as the that of the insulation (①→②). The absolute humidity of the ventilation layer (and fibrous insulation material) decreases because the indoor air actually circulates through the ventilation layer (② → ③). As a result, a water potential difference (between ① and ③) occurs between the room and the ventilation layer, causing moisture to flow from the interior to the ventilation layer. On the other hand, at night, because the thermal insulation material absorbs moisture in accordance with the decrease of the outside air temperature, the absolute humidity in the wall, including in the ventilation layer, decreases (③→④) and the water potential is maintained at a lower state in the wall than in the room. Thus, water vapor is transferred into the wall from the room due to the water potential difference (between ① and ④), so the absolute humidity gradually increases (④→①). In the periodic steady state of a one-day cycle, the above process is repeated. Due to the solar radiation received during the daytime and the advection of indoor air into the ventilation layer, moisture is discharged from the inside the wall to outside, allowing moisture permeation (dehumidification) throughout the day from the room to the inside of the wall.

Analysis of water potential behavior in the ventilation layer

The behavior of the water potential in this system was analyzed by performing a Hygrabe (Ozaki et al., 2004) numerical simulation using the unsteady heat transfer calculation tool. Table 1 lists the calculation conditions, while Figure 4 shows the roof construction and ventilation route. The roof was assumed to be on the south side of the building and to have an inclination angle of 22.4°. The calculations were performed by introducing indoor air into the ventilation layer. The building was treated as being located in Fukuoka city, Fukuoka prefecture, and the weather conditions were obtained from Extended AMeDAS weather data. The room was set to have a temperature of 27°C and a relative humidity of 70%.

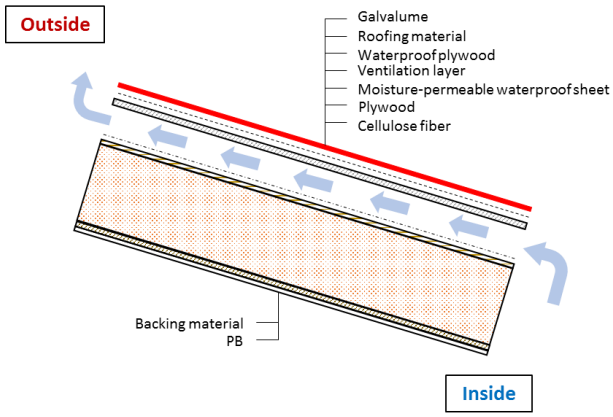

Figure 4: Roof configuration and ventilation route.

Table 1: Calculation conditions

Condition	Case 1	Case 2
Fibrous insulation material	Yes	No
Ventilation route	Room→Ventilation layer→Outside	
Flow velocity	0.2 m/s (Only from 9:00 to 17:00)	
Weather conditions	Extended AMeDAS weather data	
Calculation period	July 24–August 31	
Calculation time interval	10 s	
Indoor conditions	27°C and 70% relative humidity, constant	
Target	South side of the roof	

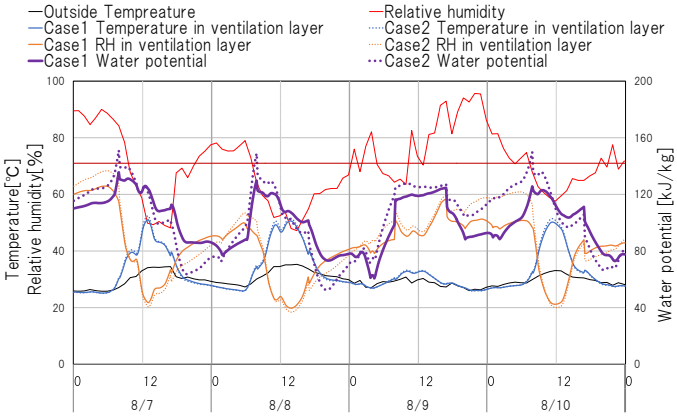

Figure 5: Temporal changes of temperature, humidity, and water potential in the ventilation layer.

Figure 5 presents the changes in the temperature, humidity, and water potential inside the ventilation layer. Although the water potential is slightly high when the ventilation begins, it gradually decreases due to the influence of the solar radiation. Moreover, by not ventilating at night, it is possible to prevent the humidity from being high in the ventilation layer, so the water

potential during the day varies less in the ventilation layer than it does indoors.

Figure 6 depicts plots of the water potential in the ventilation layer with and without fibrous insulation, which exhibit differences from one another. Upon receiving solar radiation, desorption from the fibrous insulation occurs and the relative humidity in the ventilation layer increases slightly, so the water potential also increases. Therefore, the differences between the trends in the two plots are considered to result from the presence or absence of fibrous insulation.

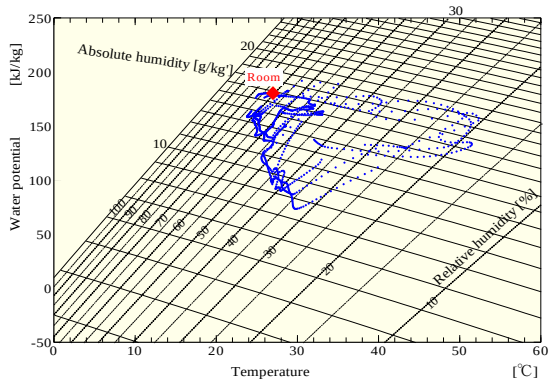

a

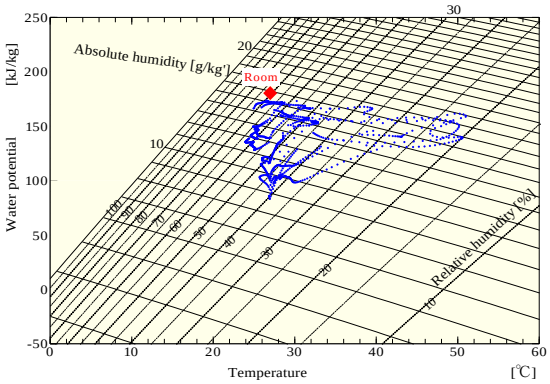

b

Figure 6: Simulated changes in the water potential in the ventilation layer over 1 month (a) without and (b) with CF insulation.

Experimental verification

Experimental setup

The characteristics of moisture transmission due to a water potential difference at constant absolute humidity were clarified by performing an experiment. A schematic diagram of the experiment is provided in Figure 7, and Figure 8 is a plan of the experimental room with the experimental apparatus. The four experimental models are numbered 1, 2, 3, and 4 along the upper part of Figure 7, and the orange rectangle in this figure is a flexible heating sheet. The room air was drawn into the instantaneous cooler through the ventilation layer in the model by the pump. Because the temperature in the instantaneous cooler could become -100°C, the amount of moisture contained in the air could be measured based on the amount of water vapor freezing in the air; thus, the amount of natural dehumidification could be obtained. The air that passed through the cooler was confirmed to be absolutely dry by using the dew point thermometer. The temperature and relative humidity of the experimental room were held constant at 27°C and 70%, respectively. Meanwhile, the temperature and humidity at the inlet of the experimental model, inside the ventilation layers and nozzle, and under the experimental model were measured using a high-performance temperature and humidity meter. Figure 9 depicts a cross-section of the

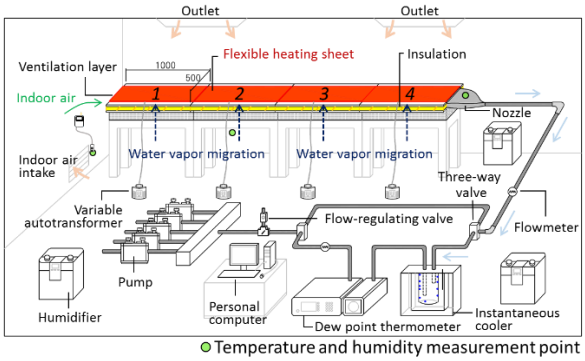

Figure 7: Schematic diagram of experimental setup.

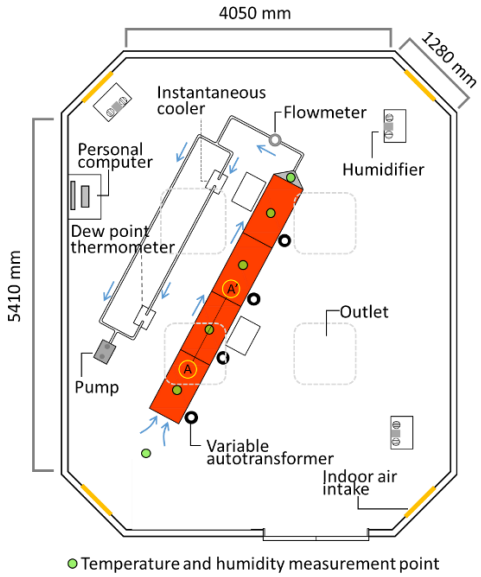

Figure 8: Plan of experimental room.

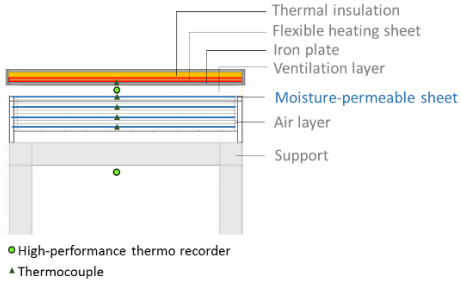

Figure 9: Cross-section of the experimental model (A-A').

experimental model. In the model, moisture-permeable sheets were installed at the bottom and could be considered thermal insulation material without moisture-storage capabilities. The air layer was formed between the moisture-permeable sheets. Iron plates with high thermal conductivity were employed externally, above the uppermost sheet. Indoor air moved through the ventilation layer formed by the cavity between the iron plate and the moisture-permeable sheets. A flexible heat sheet of the type used for floor heating was placed on the iron plate to heat the ventilation layer. Water vapor was transferred from the room to the ventilation layer through the sheet during heating. The occurrence of dehumidification was evidenced by the increases in the moisture transmitted through the sheets and the air exhausted by the pump. The surface temperatures of the iron plate and moisture-permeable sheets were measured by thermocouples.

Using these conditions, the experiment was implemented by performing the following steps.

- First, the indoor air was caused to flow into the instantaneous cooler through the ventilation layer by the pump without heating the flexible heat sheet. The temperature and humidity in the nozzle were measured and recorded during that time.
- Secondly, to simulate the structure receiving solar radiation, the flexible heating sheet was heated. Then, a water potential difference occurred between the inside of the ventilation layer and the underside of the moisture-permeable sheet, and the moisture moved from the underside to the ventilation layer. In that state, the indoor air was moved into the instantaneous cooler through the ventilation layer by the pump. The temperature and humidity were measured during that time, and the difference between the absolute humidities before and after heating the flexible heating sheet was considered to be the amount of natural dehumidification.

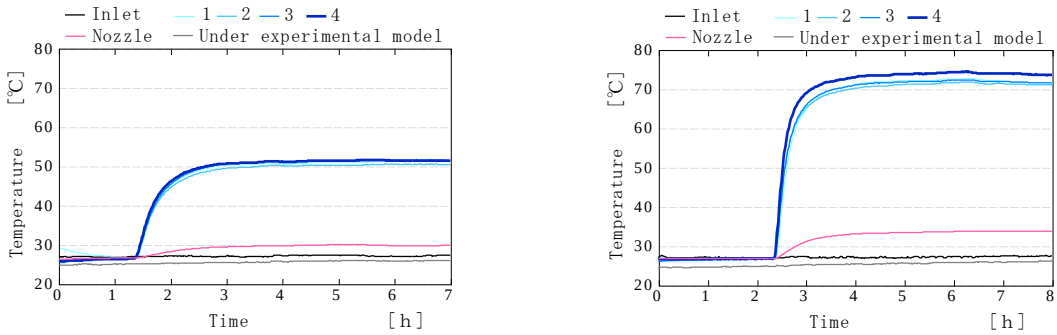

Figure 10: Temperature inside the ventilation layer with the autotransformer voltage set to (a) 50 V and (b) 100 V.

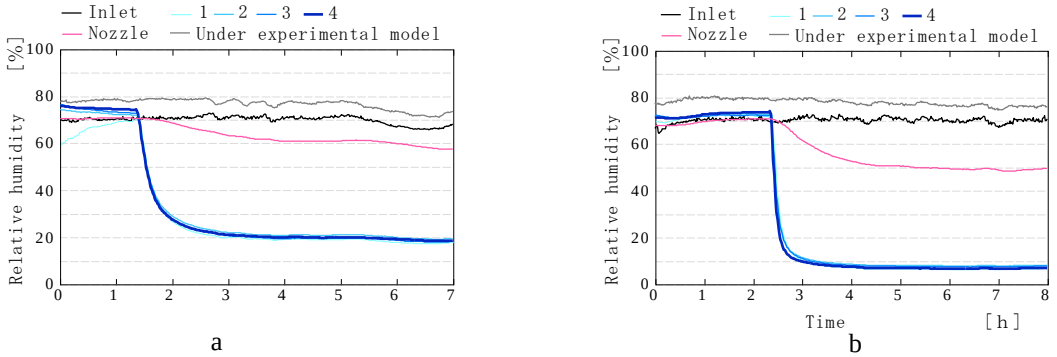

Figure 11: Relative humidity inside the ventilation layer with the autotransformer voltage set to (a) 50 V and (b) 100 V.

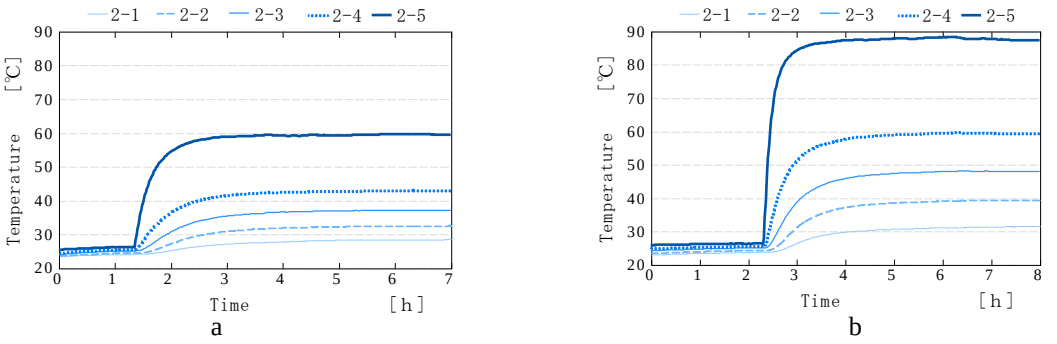

Figure 12: Temperature of the second experimental model with the autotransformer voltage set to (a) 50 V and (b) 100 V.

- Thirdly, a controlled experiment was conducted in which the temperature variations of the ventilation layer were investigated assuming that the moisture permeance remained constant due to changes in the water potential between the ventilation layer and the room to verify whether the flow-through of water vapor was proportional to the water potential difference. By changing the autotransformer voltage, the temperature of the ventilation layer was controlled and the results obtained before and after changing the voltage were examined.

Experimental results

The experiment was conducted by setting the voltage of the variable autotransformer to 50 V and 100 V. The flow rate was held constant at 0.6 m^3/h. Figures 10 and 11 present the changes in temperature and humidity under the experimental model, at the inlet of the experimental model, and inside the nozzle and ventilation layer, where the numbers 1, 2, 3, and 4 correspond to the numbered models in Figure 7.

Upon heating of the flexible heating sheet, the temperature increases and the relative humidity decreases in the ventilation layer and the nozzle. Figure 12 shows the temperature changes of the second experimental model. In the legends, 2-1, 2-2, 2-3, and 2-4 indicate the locations of the corresponding moisture-permeable sheets relative to the bottom where 2-1 denotes closest from the bottom and 2-4 denotes farthest from the bottom, respectively, while 2-5 corresponds to the iron plate underneath the flexible heating sheet. The temperature in the ventilation layer that is presented in Figure 10 can be interpreted as the average of the surface temperatures of the iron plate and the uppermost sheet.

Accuracy verification of simulated and calculated dehumidification rates

The experimental results were verified by using Hygrabe simulation software. Figures 13 and 14 present the results of a simulation of the second experiment model. The simulation results agree well with the measured results, reflecting the high precision of the Hygrabe simulation

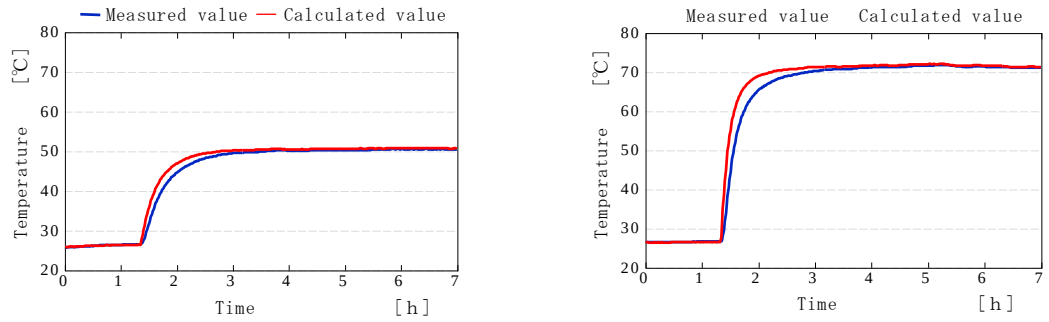

Figure 13: Temperature inside the ventilation layer in the second experimental model with the autotransformer voltage set to (a) 50 V and (b) 100 V.

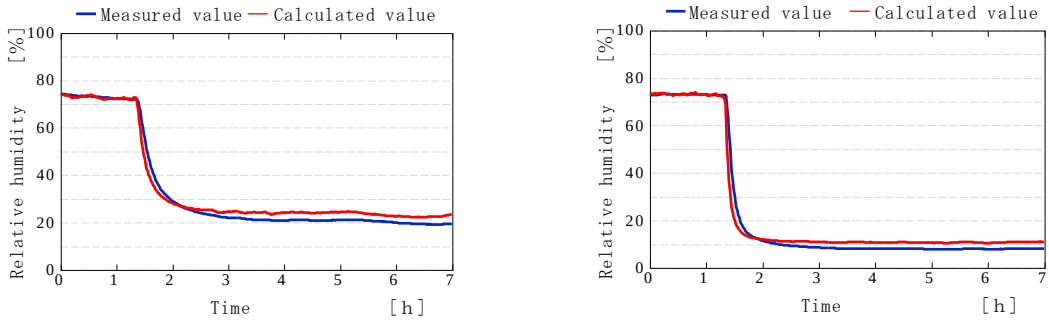

Figure 14: Relative humidity inside the ventilation layer in the second experiment model with the autotransformer voltage set to (a) 50 V and (b) 100 V.

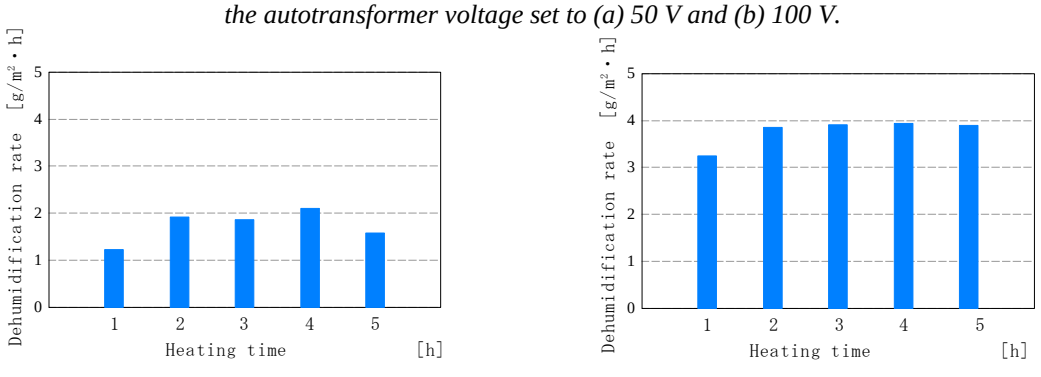

Figure 15: Dehumidification rates obtained with the autotransformer voltage set to (a) 50 V and (b) 100 V.

software. The response speed of the measurement instrument is considered to have caused the measured temperatures to increase slightly later than t0he calculated temperatures. The amount of dehumidification was calculated by taking the difference between the absolute humidities at the inlet in the experimental model and in the ventilation layer in the second model during heating based on the simulation results. Figure 15 presents the simulated dehumidification rates per unit area per hour over 5 h. The total amounts of dehumidification during the 5 h heating period were determined to be 8.7061 g and 18.8228 g when the autotransformer voltage was set to 50 V and 100 V, respectively. Therefore, the system is more effective during the day when the amount of solar radiation is higher, and the amount of dehumidification increases as the water potential difference increases.

Numerical simulation of a detached house

Calculation of dehumidification amounts in the wall and on the roof surface

Parameter sensitivity analysis related to the dehumidification of the wall was performed. Tables 1 and 2 describe the compositions and calculation conditions, respectively, of the wall and roof. Example parameter sensitivity analysis results are presented in Figure 16. Moisture absorption from and desorption into the room are represented by positive and negative values, respectively. The amount of moisture released into the room decreases in proportion to the flow rate. More moisture is absorbed from the room when the air flow is less than 0.2 m/s than when it is greater than 0.3 m/s. It is considered that the air temperature was prevented from increasing in the ventilation layer.

Table 2: Wall and roof compositions

Wall composition	**Roof composition**
Siding	Galvalume
Waterproof plywood	Roofing material
Ventilation layer	Waterproof plywood
Moisture-permeable and waterproof sheets	Ventilation layer
Structural plywood	Moisture-permeable and airtight sheets
CFs	Structural plywood
Base material	CFs
Plaster board	Backing material
	Plaster board

Table 3: Calculation conditions

Condition	**Overview**
Calculation object	South-facing wall and roof
Meteorological data	Expanded AMeDAS weather data (Fukuoka)
Calculation software	Hygrabe
Preliminary calculation	15 days
Computation period	July 20–August 19
Indoor temperature and relative humidity	27°C and 70% (constant)
Solar absorptivity	0.7
	Parameter
Ventilation	Yes (time: 9:00-16:00, 10:00-17:00, 11:00-18:00, 12:00-19:00), No
Insulation water capacity	0, CF, CF′
Interior material water conductivity	Low, Standard value, High
Flow rate in ventilation layer	0.1, 0.2, 0.3, 0.4, 0.5 m/s

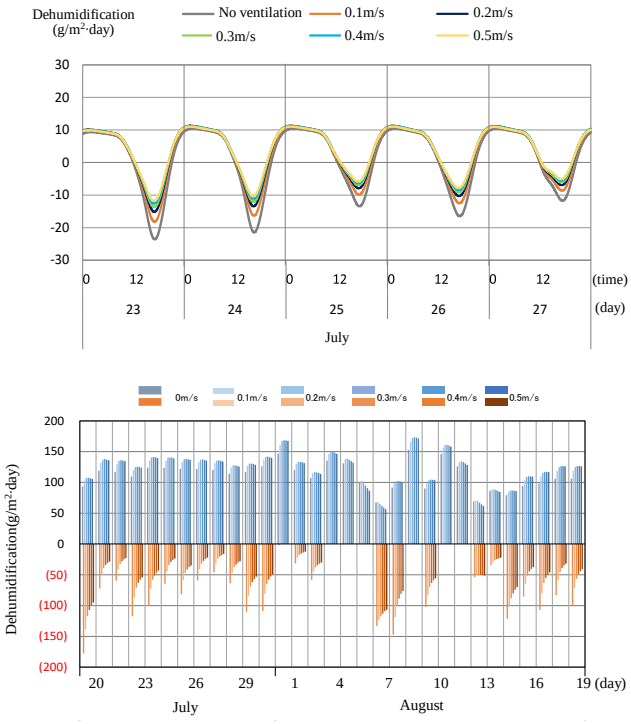

Figure 16: Influence of flow velocity on dehumidification.

Latent heat load reduction

The calculated dehumidification amounts presented above were compared with the amounts of water vapor entering the room. The water vapor was evaluated based on the indoor absolute humidity, ambient air absolute humidity, and specific gravity of the ambient air to verify the latent heat load reduction capabilities of this system. An IBEC standard house was used for the calculation model. This model is depicted in Figure 17, and its parameters are listed in Table 4. This house is highly insulated, and its thermal performance follows the Energy Conservation Standard for Housing in Japan (IBEC, 2007). The amounts of dehumidification and latent heat load reduction are presented in Figure 18. CF thermal insulation material, which is able to hold moisture, and a flow rate of 0.2 m/s were used for the calculations.

Figure 17: South side of the house model.

Table 4: Parameters of the house model

Total floor space	120.07 m^2	
Floor height	2.825 m	
Area of system	Wall	10.20 m^2
	Roof	31.77 m^2

Comparison of the moisture absorption and desorption in the wall containing CF insulation with the water vapor content in the room from the outside indicated that dehumidification of 50% or more was realized. The high dehumidification was obtained by reducing the moisture capacity of the wall by employing CF insulation, which increased the amount of moisture desorbed from the wall during the daytime due to its high moisture-holding capacity.

Conclusion

The results presented in this report demonstrate that the proposed PDSC envelope system can reduce latent heat loads by dehumidification in summer using the solar thermal energy received by the external walls and roof. The effectiveness of and dehumidification achievable by this system were confirmed by performing laboratory experiments and numerical simulations using Hygrabe hygrothermal analysis simulation software for building

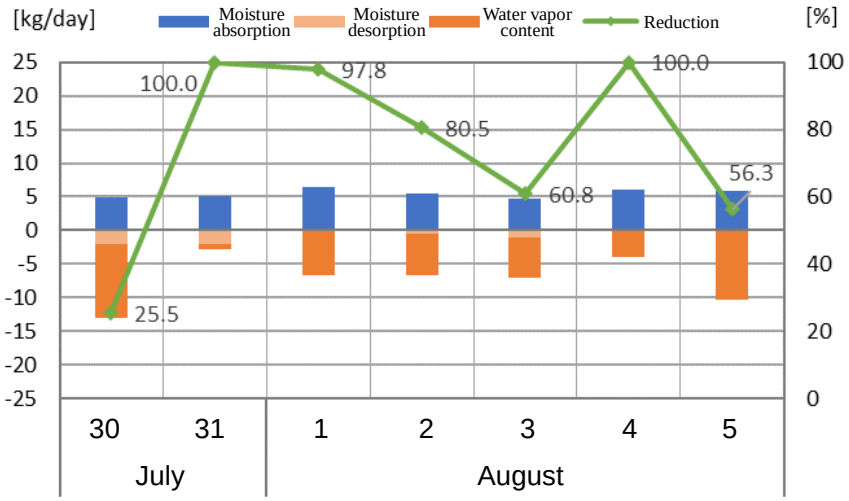

a

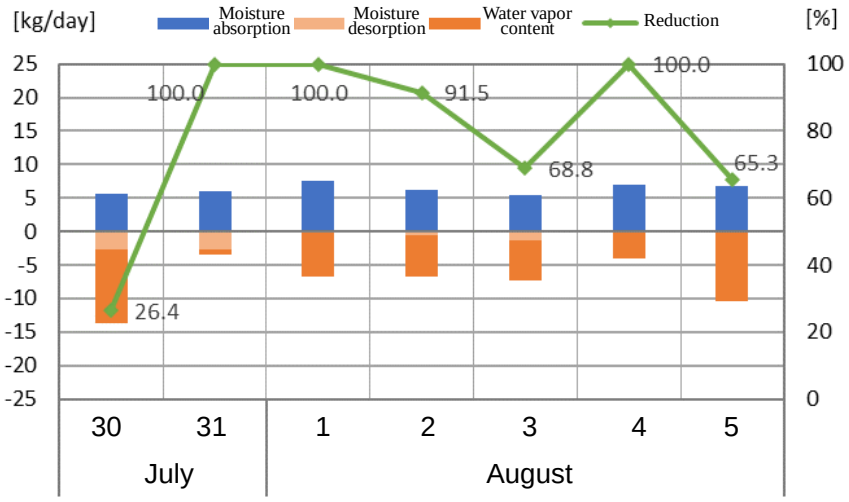

b

Figure 18: Latent heat load reduction corresponding to solar absorptivities of (a) 0.7 and (b) 0.9.

envelopes. The high precision of Hygrabe was also confirmed by the agreement between the measured and calculated results.

The air contains the transmitted moisture after passing through the ventilation layer in the experimental model. It remains necessary to confirm the dehumidification capabilities of the experimental model by actually measuring the amount of ice formed as the air passes the instantaneous cooler since the amounts of dehumidification were calculated based on the temperatures and relative humidities measured by the high-performance temperature and humidity sensor installed at the entrance of the ventilation layer in this study. Moreover, because the amounts of dehumidification in the walls and roof have only been addressed for certain indoor conditions thus far, further investigations in which actual indoor conditions, such as moisture generated inside the room, are considered are necessary for cases in which the ventilation layer thickness or insulation thickness is changed.

References

Areemit, N. and Y. Sakamoto (2006). Numerical and experimental analysis of a passive room-dehumidifying system using the sorption property of wooden attic space, *Energy and Buildings 39*, 317–327.

Lee, H., et al. (2016). Performance evaluation on dew proofing and humidity conditioning of exterior walls with characteristics of moisture absorption and desorption. *ICHES 2016, The Fifth International Conference on Human-Environment System, 20052*

Mazzi, P., et al. (2004). HVAC dehumidification system for thermal comfort: A critical review, *Applied Thermal Engineering 25*, 677–707.

Misha. S., et al. (2015). Performance of a solar assisted solid desiccant dryer for kenaf core fiber drying under low solar radiation, *Solar Energy 112*, 194–204.

METI Agency for Natural Resources and Energy (2014). Energy White Paper 2014.

IBEC (2007), Handbook of the Next Generation Energy Conservation Standard, *Institute for Building Environment and Energy Conservation*.

Ozaki, A. (2005). Heat and mass transfer of multicomponent system. *35th Symposium on Thermal Environment, Subcommittee on Thermal Environment under Research Committee on Environmental Engineering, AIJ*, 51–60.

Ozaki, A., et al. (1996). Analysis of moisture transfer by water potential: Driving force of moisture flux. *Journal of Architecture, Planning and Environmental Engineering 488*, 17–24.

Ozaki, A., T. Watanabe, and S. Takase (2004). Simulation software of the hygrothermal environment of buildings based on detailed thermodynamic models. *eSim 2004 of the Canadian Conference on Building Energy Simulation*, 45–54.

Zhang, L. (2011). An analytical solution to heat and mass transfer in hollow fiber membrane contactors for liquid desiccant air dehumidification, *Journal of Heat Transfer 133*, 092001.